Rapid Growth of a Single-Walled Carbon Nanotube on an Iron Cluster: Density-Functional Tight-Binding Molecular Dynamics Simulations

Yasuhito Ohta,[†] Yoshiko Okamoto,[†] Stephan Irle,[†,‡,*] and Keiji Morokuma[†,*]

[†]Fukui Institute for Fundamental Chemistry, Kyoto University, Kyoto 606-8103, Japan, and [‡]Institute for Advanced Research and Department of Chemistry, Nagoya University, Nagoya 464-8602, Japan

ABSTRACT Continued growth of a single-walled carbon nanotube (SWNT) on an Fe cluster at 1500 K is demonstrated using quantum chemical molecular dynamics simulations based on the self-consistent-charge density-functional tight-binding (SCC-DFTB) method. In order to deal with charge transfer between carbon and metal particles and the multitude of electronic states, a finite electronic temperature approach is applied. We present trajectories of 45 ps length, where a continuous supply of carbon atoms is directed toward the C—Fe boundary between a 7.2 Å long armchair (5,5) SWNT fragment and an attached Fe_{38} cluster. The incident carbon atoms react readily at the C—Fe interface to form C- and C_2-extensions on the tube rim that attach to the Fe cluster. These bridging sp-hybridized carbon fragments are vibrationally excited and highly mobile and, therefore, become engaged in frequent bond formation and breaking processes between their constituent C and the Fe atoms. The sp-hybridized carbon bridge dynamics and their reactions with the Fe-attached nanotube end bring about formations of new five-, six-, and seven-membered carbon rings extending the tube sidewall, resulting in overall continued growth of the nanotube on the Fe cluster up to nearly twice its length. Due to the random nature of new polygon formation, sidewall growth is observed as an irregular process without clear SWNT chirality preference. Compared to fullerene formation, heptagon formation is considerably promoted.

KEYWORDS: quantum chemical molecular dynamics simulations · density-functional tight-binding · self-assembly · continued carbon nanotube growth · iron catalyst nanoparticle · nonequilibrium dynamics

As archetypical nanotechnology materials, single-walled carbon nanotubes[1] (SWNTs) have been intensively studied since their discovery because they possess a variety of outstanding physicochemical properties[2,3] which are expected to be utilized in various potential technological applications. A large number of experimental studies have been reported on the synthesis of SWNTs,[4,5] where transition metals such as Fe, Co, Ni, Y, Mo, or binary or ternary compounds thereof are typically used as catalysts. The metal catalyst is believed to play an essential role in the nucleation and growth of SWNTs.[6] The carbon source is supplied in an inert gas atmosphere[7] either in the form of elemental carbon (laser evaporation,[8] carbon arc[9]) or in the form of hydrocarbons,[10] alcohol,[11] or CO[12] using catalytic chemical vapor deposition (CCVD) techniques. The currently widely accepted mechanism of SWNT formation is composed of three fundamental steps: (i) generation of free carbon, (ii) dissolution of carbon atoms into the metal catalyst to form a metal carbide, and (iii) precipitation of carbon on the surface of the metal catalyst, leading eventually to the growth of a cylinder-shaped nanotube. This mechanism is also frequently referred to as vapor—liquid—solid (VLS) model.[13] However, the fact that various conditions exist under which SWNTs can be synthesized may imply that their growth mechanism is not always the same or that it may be composed of multiple key reaction processes requiring different conditions for the nucleation and growth processes.[14]

Since, presently, only up to millimeter long tubes without clear chirality control can be produced, Smalley *et al.* had worked on experiments which focused on the continued growth of chirality-specific SWNTs. In 2006, Smalley's team led by Jim Tour reported a successful technique to attach iron particles to open-ended seed SWNTs and showed that continued growth can be achieved, effectively amplifying the length of the original seed tube while maintaining diameter and tube chirality.[15] While the experiment is clearly ground-breaking in its achievement, the fact remains that the reaction dynamics involving nanotube, metal catalyst, and gas-phase carbon precursor are not yet fully understood.

Exploration of such complicated nonequilibrium processes at high temperature has been a challenging issue, as experimen-

Ⓦ This paper contains enhanced objects available on the Internet at http://pubs.acs.org/journals/ancac3.

*Address correspondence to sirle@iar.nagoya-u.ac.jp, morokuma@fukui.kyoto-u.ac.jp.

Received for review March 26, 2008 and accepted June 11, 2008.

Published online June 28, 2008.
10.1021/nn8001906 CCC: $40.75

tally little is known about the reaction steps involved, or even the exact composition of the metal particles in their catalytic active state. On the theoretical/computational side, thus far, mainly Brenner's reactive empirical bond order (REBO)-type molecular mechanics methods allowing bond breaking/formation have been employed in molecular dynamics (MD) simulations of the growth process of carbon nanotubes. We list a small number of such studies in refs 16–20. However, REBO-based approaches lack quantum mechanical treatment of electrons and cannot describe important quantum mechanical phenomena such as π-conjugation or aromatic stabilization (not linearly dependent on the size of the π-system, important for sp^2-hybridized carbon) nor the effect of near-degeneracy of metal d-orbitals (important for the catalyst). We have found in the context of fullerene formation that the dynamics and mechanisms observed during MD based on the REBO potential are very different from those obtained using quantum chemical method-based molecular dynamics (QM/MD) simulations.[21] Common to direct QM/MD-type methods[22–29] is that they evaluate at every MD time step the force acting on each atom at the QM electronic structure level, which naturally includes electronic effects. Because of the QM treatment of electrons, the QM/MD method is capable of describing reaction processes which involve bond formation and breaking events and naturally includes π-conjugation effects or aromatic ring stability as well as near-degeneracy of metal d-electrons. The computational cost of QM/MD approaches depends on the approximation level of the electronic structure calculations employed.

Recently, the nucleation process of a nanotube on an iron transition metal cluster has been investigated by the first-principle MD method based on the Car–Parrinello (CPMD) approach.[30,31] However, the reported studies are inadequate because of short simulation time (due to high computational cost) and unrealistic initial model geometries. For instance, in ref 30, a nanodiamond was used as initial carbon complex, which cannot be expected to be stable under experimental SWNT synthesis condition; in fact, the same group reported that the nanodiamond transforms rapidly to an sp^2-network structure under the conditions of the study even without the presence of the metal catalyst.[32] For a thorough exploration of SWNT growth conditions, computationally less expensive methods are required that nevertheless are capable of dealing with the complicated electronic structure of transition metal clusters.

The DFTB/MD (density-functional tight-binding molecular dynamics) approach is a QM/MD technique based on the DFTB electronic structure method, a tight-binding method using an approximate density-functional formalism.[33–35] The DFTB method is approximately 2 orders of magnitude faster than first-principles density-functional theory (DFT) and therefore enables longer simulations and more adequate model systems for nonequilibrium dynamics of nanosized clusters. On the basis of such DFTB/MD simulations, we previously suggested the "shrinking hot giant" road of fullerene formation,[21] which has recently been partially confirmed by a transmission electron microscopy study[36] and mass spectroscopy of unannealed fullerenes.[37] Since many similarities should exist between fullerenes and carbon nanotubes concerning their formation mechanisms and structural features, we expect that the DFTB/MD method is also suitable for the study of the transition-metal-catalyzed SWNT nucleation and growth mechanism. With the transition metal parameters we recently published,[38] we already performed QM/MD simulations of Fe atoms attached to the open ends of a short SWNT and demonstrated that DFTB/MD gives a qualitative accurate picture compared to conventional DFT.[39]

In the present study, we have investigated the continued growth process of SWNTs on an Fe_{38} cluster using the self-consistent-charge DFTB/MD (SCC-DFTB/MD) method.[34] In the growth simulations, we focused on the reaction dynamics between feedstock carbon atoms and the Fe cluster with a short (5,5) seed SWNT attached, in the spirit of the Smalley group's experimental "continued growth".[15] By supplying C atoms around the SWNT C–Fe interface of the nanotube–Fe cluster, we have observed clear growth of the seed nanotube in QM/MD simulations. The growth process exhibits a variety of reaction processes between the nanotube–metal cluster complex and the incident C atoms. In this work, we will report the delicate interplay among the gas-phase carbon precursor, the nanotube rim, and the Fe cluster, which leads to the continued growth of the nanotube on the Fe cluster. Use of C_2 molecules instead of C atoms with the same feeding rate resulted in longer polyyne chains and associated highly disorganized growth, subsequently leading to catalyst encapsulation. To prevent this from happening, the feeding time for C_2 molecules should be increased several times, which was computationally not feasible.

RESULTS AND DISCUSSION

The Model System. Figure 1 shows our initial model system for continued growth simulations of a short SWNT fragment attached to an iron cluster. The open-ended (5,5) armchair-type nanotube is used as a seed tube with a length of 7.2 Å and a diameter of 6.7 Å, containing 60 carbon atoms. Seed tubes with different chiralities such as (8,0) zigzag-type have also been used, but due to space limitations, these results will be presented elsewhere. One end of the nanotube seed is covalently attached to a truncated octahedron Fe_{38} cluster, which is chosen to possess fcc (face centered cubic) arrangement corresponding to the stable high-temperature

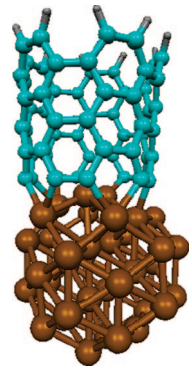

Figure 1. Model structure for the growth of a seed nanotube on an iron cluster. The (5,5) armchair carbon nanotube is attached to the Fe_{38} cluster where gray, cyan, and brown spheres represent hydrogen, carbon, and iron, respectively. The Cartesian coordinates of this structure are given in the Supporting Information.

phase of iron.[40] The end of the nanotube on the opposite side of the metal cluster is terminated by 10 H atoms to saturate dangling bonds. In an experiment, usually both ends of the nanotube are covered by a metal particle,[15] but here we truncated the tube to save computer time. The Cartesian coordinates of this end's terminal C and H atoms are frozen during the simulations to avoid reactions between incident gas-phase C atoms and the terminating H atoms that are not present in the experiment. The Cartesian coordinates of this starting structure are given in the Supporting Information. Although SCC-DFTB/MD calculations are computationally approximately 2 orders of magnitude less expensive than first-principles MD simulations, the inclusion of 38 metal atoms imposes high computational cost on the simulations. Therefore, the selection of a relatively small size of the metal cluster (~0.7 nm diameter particles are small for usual experimental conditions) and the similarly small nanotube in the present study were due to the high computational cost of the SCC-DFTB/MD simulations.

Molecular Dynamics Simulations. Starting with the initial geometry shown in Figure 1, at first, the nanotube−Fe cluster complex was annealed at 1500 K for 10 ps, and 10 geometries and associated velocities were randomly chosen from this trajectory between 5 and 10 ps for initiating the actual MD simulations. During these production "growth simulations", individual C atoms were supplied around the C−Fe interface of the nanotube−Fe cluster repeatedly with a time interval of $t_s = 0.5$ ps. The magnitude of the incident energy of the supplied carbon atom was set to 0.13 eV, which corresponds to the kinetic energy equivalent to the atomic nuclear temperature of 1500 K, and the velocity vector was directed to the position of a C atom each time randomly chosen from the C atoms forming the nanotube−Fe interface. Simulations using an incident velocity distribution instead of a fixed incident velocity are currently ongoing. A figure depicting representative random initial positions for the supplied carbon atoms around the metal−carbon interface is given in Figure S1 (Supporting Information). We added a total of 90 carbon atoms to the SWNTs and ran trajectories for a total simulation time length of 45 ps.

We have performed MD simulations for the nuclear temperature of $T_n = 1500$ K. As is discussed in detail in the Methods section, we considered the use of electronic temperature T_e in the electronic structure calculations. The electronic temperature allows fractional occupancies for molecular orbitals and takes into account the near-degeneracy of transition metal d-orbitals, which is essential in this growth mechanism. We adopted the combination of $T_e = 10\,000$ K/T_n = 1500 K and $T_e = 1500$ K/$T_n = 1500$ K. Applying $T_e = T_n$ during simulations led to similar growth behavior compared to $T_e = 10\,000$ K; therefore, in this work, we will only discuss in detail the results of the $T_e = 10\,000$ K/$T_n = 1500$ K simulations. The 10 trajectories thus executed are identified by Roman letters A to J.

Figure 2a depicts the evolved structures of the 10 trajectories after 45 ps. With different degrees of regularities, defects, and shapes, most of them clearly show substantial growth of the carbon nanotube from the seed. Characteristics for the growth in trajectory F can be seen in Figure 2b,c, and its details are given in the Supporting Information in the form of a series of Cartesian coordinates as well as in the form of a web enhanced object (WEO). The growth of the nanotube was measured by the quantity $|G_C - G_{Fe}| - r$, where G_C is the center of mass (COM) of the 10 frozen carbon atoms at the end of the nanotube opposite to the metal cluster, G_{Fe} is the COM of the Fe_{38} cluster, and r is the average radius of Fe_{38}, which was assumed to be 3.6 Å.

Growth Time Scale. The growth rate of the nanotube in the present simulation can be expected to depend on the supply interval of carbon atoms t_s. The hypothetical maximum can be estimated by assuming that all supplied carbon atoms are immediately incorporated into the nanotube hexagon network; 10 carbon atoms supplied in $t_s \times 10 = 5$ ps increase the tube length of the (5,5) nanotube by $R_{CC} \times \cos(30°) = 1.42$ Å $\times \sqrt{3}/2 = 1.23$ Å, resulting in a maximum growth rate of 0.25 Å/ps. The actual growth rate of the nanotube can be calculated from the slope of a length histogram, such as shown in Figure 2b. From the 10 trajectories studied, the average growth rate is estimated to be about 0.043 Å/ps, which is only about 1 order of magnitude slower than that of the maximum achievable rate. This finding suggests that the growth of SWNTs is rather efficient when carbon atoms are supplied directly to the metal−carbon boundary of the present system, with carbon atoms usually hitting the metal cluster first but spending relatively short time there before diffusing rather quickly to the metal-attached SWNT opening. The diameter of the tube is increased slightly to considerably, depending on the trajectory, and never decreases.

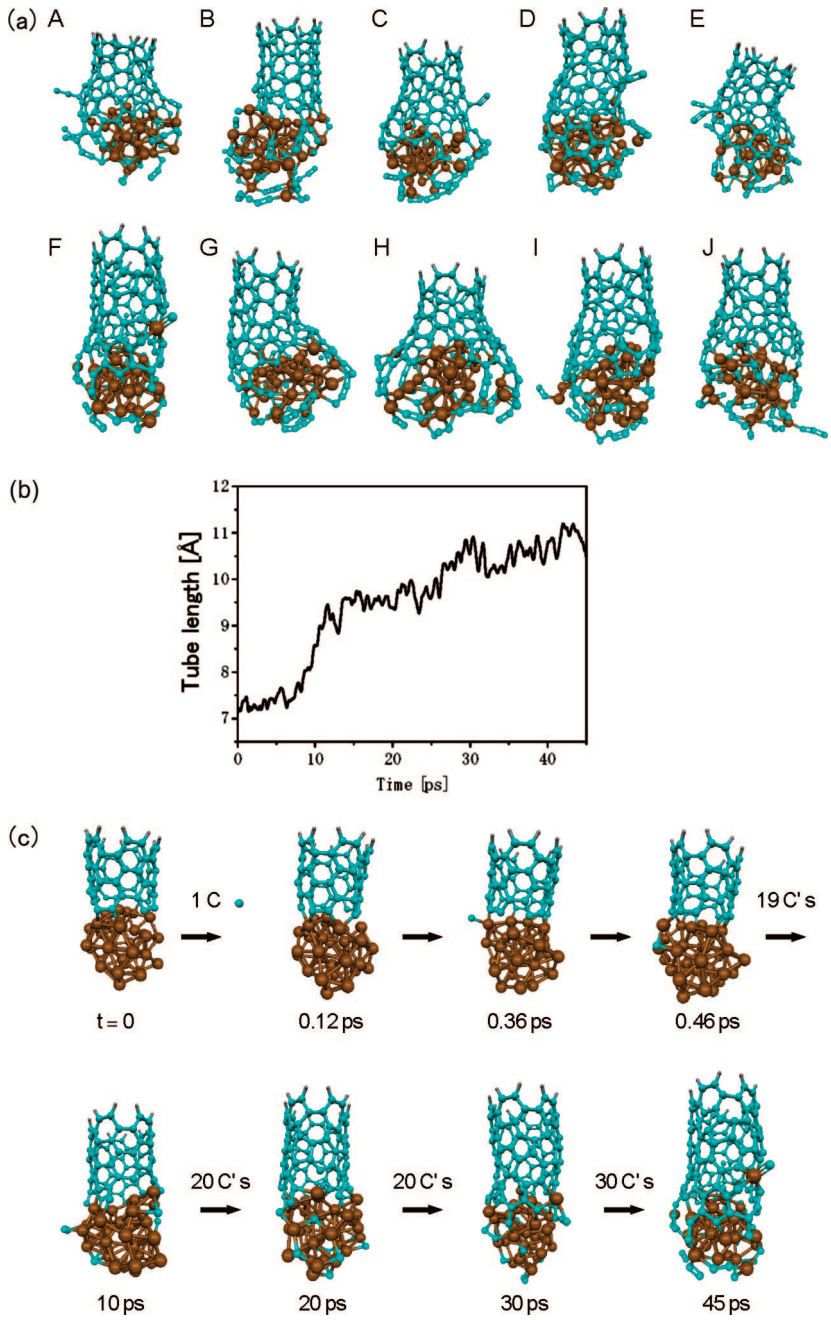

Figure 2. Growth process of a seed nanotube on an Fe_{38} cluster. (a) Structures of 10 trajectories after 45 ps simulation. For trajectory F, (b) length of the nanotube *versus* time and (c) snapshots of trajectory F at relevant intervals.

Ⓦ A movie in AVI format, video 1 is available.

Of course, it is not meaningful to compare this rate with the experimental value of $\sim 10^{-5}$ Å/ps,[5] which is 3 orders of magnitude smaller than our observed rate. Obviously, we are oversimplifying the growth process. Most significantly, we are supplying carbon *atoms* at *short intervals* to the *metal−carbon boundary*. In practice, carbon source is typically supplied in the form of small carbon molecules (C_2, C_3) which are less reactive than carbon atoms (elemental carbon processes) or as hydrocarbons where hydrogen atoms first need to be abstracted (CCVD processes). Second, the probability of supplied carbon for a direct hit of the metal−carbon boundary (which has a small cross section) can be expected to be very small; most of the carbon will instead collide with the metal cluster surface and diffuse on the surface or inside the metal cluster to reach the metal−carbon boundary and react; this diffusion process would be substantially slower that the direct reaction. This point will be discussed again in a later section.

Defects. The "grown areas" of the nanotubes contain several types of carbon polygons such as five-, six-, seven-, and even eight-membered rings, indicating the introduction of defects in the sidewall. In the snapshots of all final structures for the T_e = 10 000 K/T_n = 1500 K simulations in Figure 2a and ring counting statistics (Table 1 and Figures S2 in the Supporting Information) it is revealed that pentagon and heptagon sidewall defects develop along in the hot area where carbon addition occurs at the metal−carbon interface. The numbers of newly created five-, six-, and seven-membered rings were comparable to each other for those trajectories which show noticeable growth of the nanotube length, while slow-growth trajectories show a significantly reduced number of hexagons with pentagons and heptagons being formed with similar probability. Formation of six-membered rings seems to be important to achieve greater tube length, which makes sense as pentagons induce concave curvature and heptagons convex curvature. The present ring count statistics differ significantly from the ones obtained in our previous fullerene formation studies.[21,41] There, continued annealing increased gradually the number of hexagons over the thermodynamically less preferable pentagons from an initial 1:1 ratio, while heptagons were found very infrequently.[41] We think that it is possible that the chirality of the colder, outer SWNT hexagon network can imprint its structural features such as diameter and chiral indices on the annealing hotter growth area, although our simulation time was too short to follow this process. To create completely annealed SWNTs, probably longer than hundreds of picoseconds simulation time would be required after the addition of the final carbon atom. Such simulations are currently in progress in our laboratory.

Carbide Formation during SWNT Growth. In the present study, we have observed the penetration of several C atoms into the subsurface area of the Fe cluster. How-

TABLE 1. Ring Statistics at 45 ps for Trajectories A−J

	number of newly created rings		
	five-ring	six-ring	seven-ring
all 10 trajectories	65	37	53
ratio	0.42	0.24	0.34
rapid-growth trajectories (B,D,F,G,I,J)	39	33	30
ratio	0.38	0.32	0.29
slow-growth trajectories (A,C,E,H)	26	4	23
ratio	0.49	0.08	0.43

ever, any noticeable reaction between the nanotube and the C atoms inside the Fe cluster did not occur because of the low mobility of the dissolved C atoms in the time scale of this study (45 ps). This indicates that subsurface diffusion is not a necessary prerequisite for the SWNT growth. However, the low diffusiveness of the dissolved C atoms does not mean that such C atoms do not contribute to the growth process of the nanotube. Much longer simulation time would be necessary in order to follow the growth of the nanotube *via* subsurface diffusion or dissolution process of C atoms. We note that a substantial number of C_2 molecules are formed in all trajectories on the metal cluster surface. The formation of C_2 from supplied C atoms on the metal surface seems to be very rapid and is inline with our previous report that Fe−C_2−Fe configurations are frequently encountered in nanotube−metal interfaces.[39]

Ring Formation Process around the Metal−Carbon Boundary. Since it is impossible to discuss each trajectory in all details, we extract the major features occurring during ring formation and present simplified schematics that nevertheless reflect actual events observed during the simulations. Figure 3a shows a very schematic depiction of typical incorporation processes of the incident C atoms into the C−Fe boundary. In step (i), the incident C atom approaches the C−Fe boundary area where the edge of the nanotube, a C-bridge, or short C chains interact with the Fe cluster. In step (ii), the insertion reaction of the incident C into the C−Fe bond (●−Fe) occurs to form a triangle structure (●−○−Fe). Once the C−C bond (●−○) is newly created, the C−C−Fe (●−○−Fe) angle immediately increases by breaking the old C−Fe bond (●−Fe), and then in step (iii), a bridging structure is constructed between the nanotube and the Fe cluster. The repetition of this insertion reaction is followed by the formation of carbon ring structures at the rim of the nanotube. In these ring formation processes, five-, six-, seven-, and eight-membered rings were created and broken repetitively by the fluctuation of the C chains and the collisions between the incident C with the C−Fe interface. Figure 3b shows a schematic depiction of a typical formation process of the six-membered ring unit. In step (i), the incident C is incorporated into the C−Fe boundary to form a bridging structure (−●−○−Fe−) through the insertion reaction as described above. In step (ii), a short C bridge experiences thermal fluctuation for a while with frequent bond breaking and formation between the constituent C atoms and Fe atoms. In step (iii), the C atoms attached to the rim occasionally approach each other and form a six-membered ring. Once created, the hexagonal structural unit remains rather stable and contributes to the construction of the sidewall of the nanotube. The formation of a five-membered ring at the rim of the nanotube also occurs in a similar manner, as shown in Figure 3c. The difference here is that the inner of the two C atoms of the C bridge reacts with an adjacent original C atom. Once a five-membered ring is formed, its pentagonal structure is robustly maintained where one constituent C at the edge of the nanotube tends to be bound to an Fe atom (○−Fe). This process resembles somewhat the self-capping mechanism of open-ended nanotubes without metal clusters attached, as we have described in ref 42.

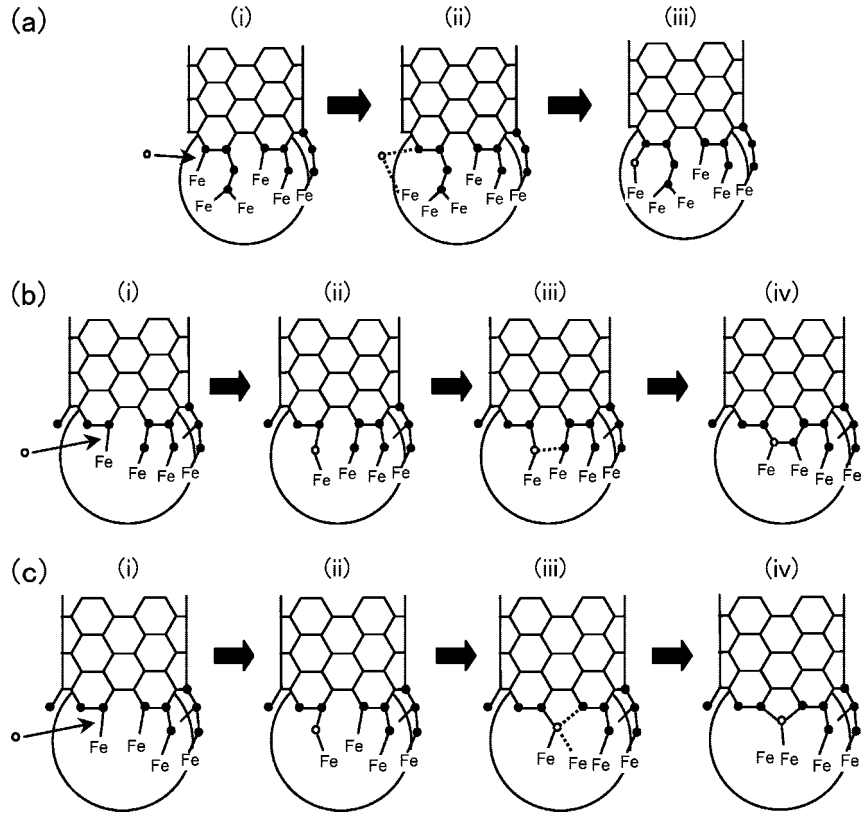

Figure 3. Schematic depictions of growth processes: (a) incorporation of the incident C into the C−Fe boundary of the nanotube−Fe cluster, (b) the six-membered ring formation, and (c) the five-membered ring formation. ○: incident C atom; ●: C atom around the C−Fe boundary.

As we had pointed out already in our DFTB/MD studies of fullerene formation, the initial pentagon/hexagon ratio is close to 1:1 at initial stages of the slab creation.[21,41] Subsequently, high temperature allows substantial slab reconstruction involving the breaking and formation of C−C bonds, and due to the thermodynamic bias toward hexagons, eventually a ratio closer to 0.33 is reached in the case of fullerene formation.[41] In the presence of the transition metal catalyst facilitating a large number of pentagons and heptagons, carbon mobility, and lower temperature of SWNT formation as opposed to the higher temperatures of fullerene formation, an even greater dominance of hexagons over pentagons can be expected toward the end of the annealing process, which possibly explains the fact that SWNTs are hexagon-only structures (except for the caps at their ends or sudden tube bents that are sometimes observed in experiment).

SUMMARY

In summary, we have demonstrated rapid growth behavior of a nanotube on an iron cluster using quantum chemical method-based molecular dynamics simulations (QM/MD) using the self-consistent-charge density-functional tight-binding (SCC-DFTB) method. By providing an abundant, targeted supply of C atoms around the C−Fe interface of a nanotube−Fe model cluster, we have observed prompt insertion of the incident C into the C−Fe boundary to form short bridging C- and C_2-extensions of the nanotube and the Fe cluster. The repetitive insertion and subsequent bridging sp-hybridized carbon fragment formation results in the rapid formation of five-, six-, seven-, and sometimes even eight-membered rings which contribute to the continued growth process of the nanotube on the Fe cluster.

We find that the presence of long polyyne chains ($n > 4$) is not a necessary prerequisite for the continued growth, and neither seems carbide formation to be a necessary requirement. Rather, the short C- and C_2-extensions on the nanotube rim that are somewhat reminiscent of the "wobbling C_2" units we had described in the self-capping process of open-ended SWNTs[42] were observed to perform the polygon construction and sidewall extension. These sp-hybridized carbon bridges are directly attached to the metal cluster, and their adhesion strength[43] could very well be important for the maintenance of the tube diameter. Our results suggest that it is possible for the nanotube to grow on the metal particle without surface or subsurface diffusion of the C atoms on the metal cluster, although we note that this finding is due to our targeting of the C−Fe interface region by the incident C atoms. Surface/subsurface diffusion of the C atoms on the metal catalyst may still be important for the growth of the nanotube due to the larger cross section for carbon−metal collisions. Pursuing such diffusion processes as well as the complete annealing of the five-, seven-, and eight-membered ring defects requires a much longer simulation time scale, and the relevant work is now in progress.

We note that clear chirality selection could not be accomplished at the carbon−metal interface due to the high exothermicity of the addition reaction, resulting in an almost equal generation of five-, six-, and seven-membered rings for rapid-growth trajectories, different from fullerene formation where mainly five- and six-membered but not six-membered ring formation is observed. In case of slow-growth trajectories, a 1:1 ratio between newly created pentagons and heptagons was observed, with a much smaller number of hexagons, linking hexagon formation to tube length. Due to the apparent random nature of new carbon polygon formation, sidewall growth appears as an irregular process without clear SWNT chirality preference. This is an interesting finding as it was speculated that the highly irregular, defective tubes "grown" in REBO simulations[16−20] are due to the lack of π-conjugation in this semiempirical potential. Our results suggest that the tube chirality observed in experimentally synthesized tubes may rather be a result of the chirality imprinted by the colder tube section (or cap) further away from the growth region during the annealing of the freshly grown sidewall area. Simulations to test this hypothesis are now ongoing.

METHODS

SCC-DFTB Method. In the present QM/MD simulations, we employed the self-consistent-charge (SCC)-DFTB method[34] for obtaining the quantum potential. The DFTB method is based on the second-order expansion of the total electronic DFT energy with respect to the variation of a reference density. In the SCC-DFTB method, the atomic charge−charge interaction is explicitly included in the electronic energy and the DFTB secular equation is solved iteratively until the Mulliken atomic charges become self-consistent with the Hamiltonian. There exists a nonconsistent charge (NCC) version of DFTB in which the atomic charge−charge interaction is completely neglected. NCC-DFTB method requires no iteration and is several times less expensive than the SCC-DFTB and was used for our previous MD studies of fullerene formation from C_2 molecules[21,41] because, in a system consisting only of carbon atoms, charge polarization can safely be neglected. However, in the present system consisting of transition metals and free-floating carbons fragments, NCC-DFTB gives a totally wrong charge distribution and should therefore not be used.

Fractional Occupation Numbers and Electronic Temperature. In the SCC-DFTB calculation, the total electronic energy E is given as

$$E = 2\sum_i \varepsilon_i f_i + E_{\text{rep}} \quad (1)$$

where the first and the second terms in eq 1 represent the so-called electronic or band structure energy and the repulsive

short-range potential, respectively, with ε_i and f_i being the orbital energy and the orbital occupation. In the simple closed shell calculation, f_i is 1 for occupied orbitals and 0 for vacant orbitals. In the present simulation, we adopted the Fermi−Dirac distribution function for f_i

$$f_i = \frac{1}{\exp[(\varepsilon_i - \mu)/k_B T_e] + 1}, \quad 0 \le f_i \le 1 \qquad (2)$$

which changes continuously from ~1 for low energy orbitals to ~0 for high energy orbitals. In this equation, k_B is the Boltzmann constant, T_e is the so-called "electronic temperature", and μ is the chemical potential, which is numerically determined so that the sum of all the fractional number of electrons is equal to the total number of electrons N_e:$N_e = 2\Sigma_i f_i$. In the fractional occupation scheme, it is well-known that the variational quantity is not the total electronic energy E but the Mermin free energy $E - T_e S_e$, where S_e is the electronic entropy. In the case of the Fermi−-Dirac function, S_e is given as[44]

$$S_e = -2k_B \sum_i^{\infty} [f_i \ln f_i + (1 - f_i)\ln(1 - f_i)] \qquad (3)$$

It should be noted that the electronic temperature need not to be equal to the nuclear temperature of the reaction system.[44–47] Several thousand Kelvin is commonly used for improving convergence in electronic structure calculations.[48] In the present study, the main purpose of using electronic temperature is to describe in an averaged and qualitative fashion the participation of many electronic states arising from the near-degeneracy of 3d-orbitals of the transition metal cluster. In this treatment, the spin of electrons is not included explicitly since the overall effect of the spin is not expected to be large for an average of many spin states generated from the fractional occupancy of many orbitals in the cluster. One advantage of the continuous change in fractional occupation number is that the electronic energy and therefore the total SCC-DFTB energy are continuous during the propagation of the trajectories, and one can avoid the energy discontinuity arising from the crossing of different states due to different occupied and vacant orbitals. Concerning the somewhat arbitrary choice of electronic temperature, we used mainly T_e = 10 000 K. The corresponding energy $k_B T_e$ ~ 0.87 eV is comparable to the half-width of the 3d band of the present Fe cluster. We have also examined the case of T_e=T_n=1500 K, where T_n is the nuclear temperature, and we confirmed that the present results were not significantly affected by the range of the electronic temperatures. If T_e is not explicitly mentioned in the text above, we discuss only the results for the case T_e =10 000 K.

It is worth mentioning that no use of fractional occupancy (or equivalently T_e = 0 K) corresponds to the adaptation of a closed shell single determinant wave function where only the lowest energy orbitals are doubly occupied up to the HOMO, while all the orbitals above the HOMO are considered vacant. Preliminary calculations indicate that assuming such a state causes serious convergence problems during the SCC iterations for each step of the MD simulations even for much smaller metal−carbon systems. Thus the use of the finite temperature approach is mandatory for the present system.

Molecular Dynamics Simulations. The molecular dynamics simulations were performed with a time step of 1.0 fs using the velocity Verlet integrator. Periodic boundary conditions were imposed with a cubic box size of 100 Å^3. The nuclear temperature of the system was kept at a target temperature of 1500 K using the Nose−Hoover chain thermostat,[49] emulating effective and frequent collisions with the inert gas.

Acknowledgment. S.I. acknowledges support by the Program for Improvement of Research Environment for Young Researchers from Special Coordination Funds for Promoting Science and Technology (SCF) commissioned by the Ministry of Education, Culture, Sports, Science and Technology (MEXT) of Japan. This work was in part supported by a CREST (Core Research for Evolutional Science and Technology) grant in the Area of High Performance Computing for Multiscale and Multiphysics Phenomena from the Japan Science and Technology Agency (JST). The simulations were performed in part using the computer resources at the Research Center for Computational Science (RCCS), Okazaki Research Facilities, National Institutes for Natural Sciences.

Supporting Information Available: Cartesian coordinates of the $Fe_{38}C_{60}H_{10}$ starting structure; a figure depicting representative random initial positions for the supplied carbon atoms around the metal−carbon interface; trajectory F corresponding to Figure 2c in form of a series of Cartesian coordinates; and ring counting statistics for all T_e = 10 00 K/T_n = 1500 K simulations during runtime. This material is available free of charge via the Internet at http://pubs.acs.org.

REFERENCES AND NOTES

1. Iijima, S.; Ichihashi, T. Single-Shell Carbon Nanotubes of 1-nm Diameter. *Nature* **1993**, *364*, 737.
2. Dresselhaus, M. S.; Dresselhaus, G.; Eklund, P. C. *Science of Fullerenes and Carbon Nanotubes*; Academic Press: New York, 1996.
3. Saito, R.; Dresselhaus, G.; Dresselhaus, M. S. *Physical Properties of Carbon Nanotube*; Imperial College Press: London, 1998.
4. Moisala, A.; Nasibulin, A. G.; Kauppinen, E. I. The Role of Metal Nanoparticles in the Catalytic Production of Single-Walled Carbon Nanotubes—A Review. *J. Phys.: Condens. Matter* **2003**, *15*, S3011−S3035.
5. Hata, K.; Futaba, D. N.; Mizuno, K.; Namai, T.; Yumura, M.; Iijima, S. Water-Assisted Highly Efficient Synthesis of Impurity-Free Single-Waited Carbon Nanotubes. *Science* **2004**, *306*, 1362–1364.
6. Journet, C.; Bernier, P. Production of Carbon Nanotubes. *Appl. Phys. A* **1998**, *67*, 1–9.
7. Nishide, D.; Kataura, H.; Suzuki, S.; Tsukagoshi, K.; Aoyagi, Y.; Achiba, Y. High-Yield Production of Single-Wall Carbon Nanotubes in Nitrogen Gas. *Chem. Phys. Lett.* **2003**, *372*, 45–50.
8. Thess, A.; Lee, R.; Nikolaev, P.; Dai, H. J.; Petit, P.; Robert, J.; Xu, C. H.; Lee, Y. H.; Kim, S. G.; Rinzler, A. G.; et al. Crystalline Ropes of Metallic Carbon Nanotubes. *Science* **1996**, *273*, 483–487.
9. Bethune, D. S.; Kiang, C. H.; Devries, M. S.; Gorman, G.; Savoy, R.; Vazquez, J.; Beyers, R. Cobalt-Catalyzed Growth of Carbon Nanotubes with Single-Atomic-Layerwalls. *Nature* **1993**, *363*, 605–607.
10. Dai, H.; Rinzler, A. G.; Nikolaev, P.; Thess, A.; Colbert, D. T.; Smalley, R. E. Single-Wall Nanotubes Produced by Metal-Catalyzed Disproportionation of Carbon Monoxide. *Chem. Phys. Lett.* **1996**, *260*, 471–475.
11. Maruyama, S.; Kojima, R.; Miyauchi, Y.; Chiashi, S.; Kohno, M. Low-Temperature Synthesis of High-Purity Single-Walled Carbon Nanotubes from Alcohol. *Chem. Phys. Lett.* **2002**, *360*, 229–234.
12. Nikolaev, P.; Bronikowski, M. J.; Bradley, R. K.; Rohmund, F.; Colbert, D. T.; Smith, K. A.; Smalley, R. E. Gas-Phase Catalytic Growth of Single-Walled Carbon Nanotubes from Carbon Monoxide. *Chem. Phys. Lett.* **1999**, *313*, 91–97.
13. Harris, P. J. F. Solid State Growth Mechanisms for Carbon Nanotubes. *Carbon* **2007**, *45*, 229–239.
14. Qi, H.; Yuan, D. N.; Liu, J. Two-Stage Growth of Single-Walled Carbon Nanotubes. *J. Phys. Chem. C* **2007**, *111*, 6158–6160.
15. Smalley, R. E.; Li, Y. B.; Moore, V. C.; Price, B. K.; Colorado, R.; Schmidt, H. K.; Hauge, R. H.; Barron, A. R.; Tour, J. M. Single Wall Carbon Nanotube Amplification: *En Route* to a Type-Specific Growth Mechanism. *J. Am. Chem. Soc.* **2006**, *128*, 15824–15829.
16. Bolton, K.; Ding, F.; Rosen, A. Atomistic Simulations of Catalyzed Carbon Nanotube Growth. *J. Nanosci. Nanotechnol.* **2006**, *6*, 1211–1224.

17. Ding, F.; Bolton, K.; Rosen, A. Nucleation and Growth of Single-Walled Carbon Nanotubes: A Molecular Dynamics Study. *J. Phys. Chem. B* **2004**, *108*, 17369–17377.
18. Ding, F.; Bolton, K.; Rosen, A. Molecular Dynamics Study of SWNT Growth on Catalyst Particles without Temperature Gradients. *Comput. Mater. Sci.* **2006**, *35*, 243–246.
19. Duan, H.; Ding, F.; Rosen, A.; Harutyunyan, A.; Tokune, T.; Curtarolo, S.; Bolton, K. Initial Growth of Single-Walled Carbon Nanotubes on Supported Iron Clusters: A Molecular Dynamics Study. *Eur. Phys. J. D* **2007**, *43*, 185–188.
20. Maruyama, S.; Shibuta, Y. Molecular Dynamics in Formation Process of SWNTs. *Mol. Cryst. Liq. Cryst.* **2002**, *387*, 87–92.
21. Irle, S.; Zheng, G.; Wang, Z.; Morokuma, K.; Elstner, M. The C60 Formation Puzzle "Solved": QM/MD Simulations Reveal the Shrinking Hot Giant Road of the Dynamic Fullerene Self-Assembly Mechanism. *J. Phys. Chem. B* **2006**, *110*, 14531–14545.
22. Car, R.; Parrinello, M. Unified Approach for Molecular-Dynamics and Density-Functional Theory. *Phys. Rev. Lett.* **1985**, *55*, 2471–2474.
23. Chen, W.; Hase, W. L.; Schlegel, H. B. *Ab-Initio* Classical Trajectory Study of $H_2CO \rightarrow H_2 + CO$ Dissociation. *Chem. Phys. Lett.* **1994**, *228*, 436–442.
24. Millam, J. M.; Bakken, V.; Chen, W.; Hase, W. L.; Schlegel, H. B. Ab-Initio Classical Trajectories on the Born−Oppenheimer Surface: Hessian-Based Integrators Using Fifth-Order Polynomial and Rational Function Fits. *J. Chem. Phys.* **1999**, *111*, 3800–3805.
25. Schlegel, H. B.; Millam, J. M.; Iyengar, S. S.; Voth, G. A.; Daniels, A. D.; Scuseria, G. E.; Frisch, M. J. *Ab-Initio* Molecular Dynamics: Propagating the Density Matrix with Gaussian Orbitals. *J. Chem. Phys.* **2001**, *114*, 9758–9763.
26. Iyengar, S. S.; Schlegel, H. B.; Millam, J. M.; Voth, G. A.; Scuseria, G. E.; Frisch, M. J. *Ab-Initio* Molecular Dynamics: Propagating the Density Matrix with Gaussian Orbitals. II. Generalizations Based on Mass-Weighting, Idempotency, Energy Conservation and Choice of Initial Conditions. *J. Chem. Phys.* **2001**, *115*, 10291–10302.
27. Iyengar, S. S.; Schlegel, H. B.; Voth, G. A. Atom-Centered Density Matrix Propagation (ADMP): Generalizations Using Bohmian Mechanics. *J. Phys. Chem. A* **2003**, *107*, 7269–7277.
28. Iyengar, S. S.; Schlegel, H. B.; Voth, G. A.; Millam, J. M.; Scuseria, G. E.; Frisch, M. J. *Ab-Initio* Molecular Dynamics: Propagating the Density Matrix with Gaussian Orbitals. IV Formal Analysis of the Deviations from Born−Oppenheimer Dynamics. *Isr. J. Chem* **2002**, *42*, 191–202.
29. Schlegel, H. B.; Iyengar, S. S.; Li, X. S.; Millam, J. M.; Voth, G. A.; Scuseria, G. E.; Frisch, M. J. *Ab-Initio* Molecular Dynamics: Propagating the Density Matrix with Gaussian Orbitals. III Comparison with Born−Oppenheimer Dynamics. *J. Chem. Phys.* **2002**, *117*, 8694–8704.
30. Raty, J. Y.; Gygi, F.; Galli, G. Growth of Carbon Nanotubes on Metal Nanoparticles: A Microscopic Mechanism from *Ab-Initio* Molecular Dynamics Simulations. *Phys. Rev. Lett.* **2005**, *95*, 096103.
31. Gavillet, J.; Thibault, J.; Stephan, O.; Amara, H.; Loiseau, A.; Bichara, C.; Gaspard, J. P.; Ducastelle, F. Nucleation and Growth of Single-Walled Nanotubes: The Role of Metallic Catalysts. *J. Nanosci. Nanotechnol.* **2004**, *4*, 346–359.
32. Raty, J. Y.; Galli, G.; Bostedt, C.; van Buuren, T. W.; Terminello, L. J. Quantum Confinement and Fullerenelike Surface Reconstructions in Nanodiamonds. *Phys. Rev. Lett.* **2003**, *90*, 037401.
33. Porezag, D.; Frauenheim, T.; Kohler, T.; Seifert, G.; Kaschner, R. Construction of Tight-Binding-Like Potentials on the Basis of Density-Functional Theory: Application to Carbon. *Phys. Rev. B* **1995**, *51*, 12947–12957.
34. Elstner, M.; Porezag, D.; Jungnickel, G.; Elsner, J.; Haugk, M.; Frauenheim, T.; Suhai, S.; Seifert, G. Self-Consistent-Charge Density-Functional Tight-Binding Method for Simulations of Complex Materials Properties. *Phys. Rev. B* **1998**, *58*, 7260–7268.
35. Frauenheim, T.; Seifert, G.; Elstner, M.; Niehaus, T.; Kohler, C.; Amkreutz, M.; Sternberg, M.; Hajnal, Z.; Di Carlo, A.; Suhai, S. Atomistic Simulations of Complex Materials: Ground-State and Excited-State Properties. *J. Phys.: Condens. Matter* **2002**, *14*, 3015–3047.
36. Huang, J. Y. Real Time Microscopy, Kinetics, and Mechanism of Giant Fullerene Evaporation. *Phys. Rev. Lett.* **2007**, *99*, 175503.
37. Bogana, M.; Ravagnan, L.; Casari, C. S.; Zivelonghi, A.; Baserga, A.; Bassi, A. L.; Bottani, C. E.; Vinati, S.; Salis, E.; Piseri, P.; et al. Leaving the Fullerene Road: Presence and Stability of sp Chains in sp^2 Carbon Clusters and Cluster-Assembled Solids. *New J. Phys.* **2005**, *7*, 81.
38. Zheng, G. S.; Witek, H. A.; Bobadova-Parvanova, P.; Irle, S.; Musaev, D. G.; Prabhakar, R.; Morokuma, K. Parameter Calibration of Transition-Metal Elements for the Spin-Polarized Self-Consistent-Charge Density-Functional Tight-Binding (DFTB) Method: Sc, Ti, Fe, Co, and Ni. *J. Chem. Theory Comput.* **2007**, *3*, 1349–1367.
39. Zheng, G.; Irle, S.; Morokuma, K. Fe/C Interactions During SWNT Growth with C2 Feedstock Molecules: A Quantum Chemical Molecular Dynamics Study. *J. Nanosci. Nanotechnol.* **2006**, *6*, 1259–1270.
40. Zhang, Q. M.; Wells, J. C.; Gong, X. G.; Zhang, Z. Y. Adsorption of a Carbon Atom on the Ni-38 Magic Cluster and Three Low-Index Nickel Surfaces: A Comparative First-Principles Study. *Phys. Rev. B* **2004**, *69*, 205413.
41. Irle, S.; Wang, Z.; Zheng, G.; Morokuma, K. "Shrinking Hot Giant" Road of Dynamic Fullerene Self-Assembly in Hot Carbon Vapor. *Nano* **2007**, *2*, 21–30.
42. Zheng, G. S.; Irle, S.; Elstner, M.; Morokuma, K. Quantum Chemical Molecular Dynamics Model Study of Fullerene Formation from Open-Ended Carbon Nanotubes. *J. Phys. Chem. A* **2004**, *108*, 3182–3194.
43. Ding, F.; Larsson, P.; Larsson, J. A.; Ahuja, R.; Duan, H. M.; Rosen, A.; Bolton, K. The Importance of Strong Carbon−Metal Adhesion for Catalytic Nucleation of Single-Walled Carbon Nanotubes. *Nano Lett.* **2008**, *8*, 463–468.
44. Weinert, M.; Davenport, J. W. Fractional Occupations and Density-Functional Energies and Forces. *Phys. Rev. B* **1992**, *45*, 13709–13712.
45. Wentzcovitch, R. M.; Martins, J. L.; Allen, P. B. Energy *versus* Free-Energy Conservation in First-Principles Molecular-Dynamics. *Phys. Rev. B* **1992**, *45*, 11372–11374.
46. Wagner, F.; Laloyaux, T.; Scheffler, M. Errors in Hellmann-Feynman Forces Due to Occupation-Number Broadening and How They Can Be Corrected. *Phys. Rev. B* **1998**, *57*, 2102–2107.
47. Koga, J.; Nishio, K.; Yamaguchi, T.; Yonezawa, F. Order N Non-Orthogonal Tight-Binding Molecular Dynamics and Its Application to the Study of Glass Transition in Germanium. *J. Phys. Soc. Jpn.* **2004**, *73*, 136–144.
48. Rabuck, A. D.; Scuseria, G. E. Improving Self-Consistent Field Convergence by Varying Occupation Numbers. *J. Chem. Phys.* **1999**, *110*, 695–700.
49. Martyna, G. J.; Klein, M. L.; Tuckerman, M. Nosé−Hoover Chains: The Canonical Ensemble *via* Continuous Dynamics. *J. Chem. Phys.* **1992**, *97*, 2635–2643.